Geology, ore characteristics, and origin of the Albany graphite deposit

Andrew G. Conly[1, a] and Lindsay C. Moore[1]

[1] Mineralogy and Experimental Laboratory, Department of Geology, Lakehead University, Thunder Bay, ON
[a] corresponding author: aconly@lakeheadu.ca

Recommended citation: Conly, A.G. and Moore, L.C., 2015. Geology, ore characteristics, and origin of the Albany graphite deposit. In: Simandl, G.J. and Neetz, M., (Eds.), Symposium on Strategic and Critical Materials Proceedings, November 13-14, 2015, Victoria, British Columbia. British Columbia Ministry of Energy and Mines, British Columbia Geological Survey Paper 2015-3, pp. 173-185.

1. Introduction

The Albany graphite deposit is a 24 Mt, low-grade, breccia-hosted graphite deposit currently under development by Zenyatta Ventures Ltd., near Hearst, Ontario (Fig. 1). The deposit was discovered following an airborne geophysical survey and subsequent exploration diamond drilling of nickel-copper-platinum group minerals targets. Between 2010 and 2014, Zenyatta Ventures confirmed a graphite deposit hosted in two large breccia pipes (hereafter referred to as the East Pipe and West Pipe) that intruded along the southern margin of an arcuate chain of Mesoproterozic to Neoproterozoic alkalic intrusions.

Studies of the Albany deposit have been lacking because of minimal exploration and mapping in the area, and due to extensive cover by Phanerozoic rocks and glacial overburden. Herein we integrate field, mineralogical, and isotopic data to document the origin of the deposit. We also document the physicochemical properties of the graphite, which is important to establish during early states of exploration to address questions about markets and commercial viability.We consider that Albany is an epigenetic, igneous-hosted, fluid-derived graphite deposit (see Luque et al., 2013 for a treatment of graphite deposits). Although uncommon relative to the syngenetic deposits, which are formed by the conversion of carbonaceous material by contact or regional metamorphism, fluid-derived deposits commonly account for the highest quality of natural graphite (Luque et al., 2013; e.g., Sri Lanka; Borrowdale, UK; Huelma, Spain; New York; Montana).

2. Geological setting

The Albany graphite deposit is in the southern Marmion terrane of the Superior Province (Fig. 1), along the southern margin of the Nagagami River Alkalic Rock complex (NRAC; Sage, 1988) and immediately north of the Gravel River fault, which separates the Marmion terrane and NRAC from the Quetico sub-province to the south (Figs. 1, 2; Kennedy, 1984). The Albany graphite deposit is hosted by the Albany Alkalic complex, which may be part of the NRAC (Figs. 2, 3). The Nagagami River and Albany complexes are the most southern in a series of intrusions that define a north- to northwest-trending arcuate band of inferred alkalic magmatism (Fig. 2).

The absolute ages of the Nagagami River and Albany complexes are unknown. The Nagagami River Alkali complex cuts north to northwesterly trending Paleoproterozoic Matachewan (Hearst) dike swarms (ca. 2454 Ma; Heaman, 1988; Phinney and Morrison, 1988) and the east-northeasterly Kapuskasing dike swarm (ca. 2124-2170; Stott, 2008; Fig. 2). Temporal reationships between dikes and the Albany Alkali complex are complicated, as dikes cut the complex and vice versa. However, it is possible that dikes cutting the complex are related to augite-aegirine sills that transect the Albany deposit at depth (Fig. 4b), which are mineralogically and chemically distinct from regional dike swarms.

Precambrian rocks in the region are unconformably overlain by muskeg, glacial till, and Paleozoic (Ordovician to Devonian) carbonate rocks of the Moose River basin (James Bay Lowlands; Johnson et al., 1991). The glacial overburden ranges from 28 to 55 m (average 44 m) and the Paleozoic cover ranges from 0 to 16 m (average 3.8 m) in thickness.

3. Deposit geology

3.1. Grade and tonnage

Zenyatta Ventures Ltd. discovered the Albany deposit in 2010 using VTEM airborne geophysical surveys that suggested a pipe-like structure. Subsequent ground geophysical surveys (large loop TDEM; Fig. 4a) in 2013, provided improved resolution, and led to the discovery of two adjacent breccia pipes (Legault et al., 2015). Diamond drilling by Zenyatta Ventures between 2010 and 2014 confirmed the existence of the breccia pipes (East and West pipes; Fig. 4b). Open pit indicated mineral resources are estimated to total 24.3 million tonnes (Mt) at an average grade of 3.98% graphitic carbon (C_g), containing 968,000 tonnes of C_g; inferred mineral resources (open pit and underground) are estimated to total 16.9 Mt at an average grade of 2.64% C_g, containing 445,000 tonnes of C_g (RPA Inc., 2015).

3.2. Host rocks

The graphite-hosting rocks of the Albany complex vary from quartz syenite to diorite to nepheline syenite, with quartz

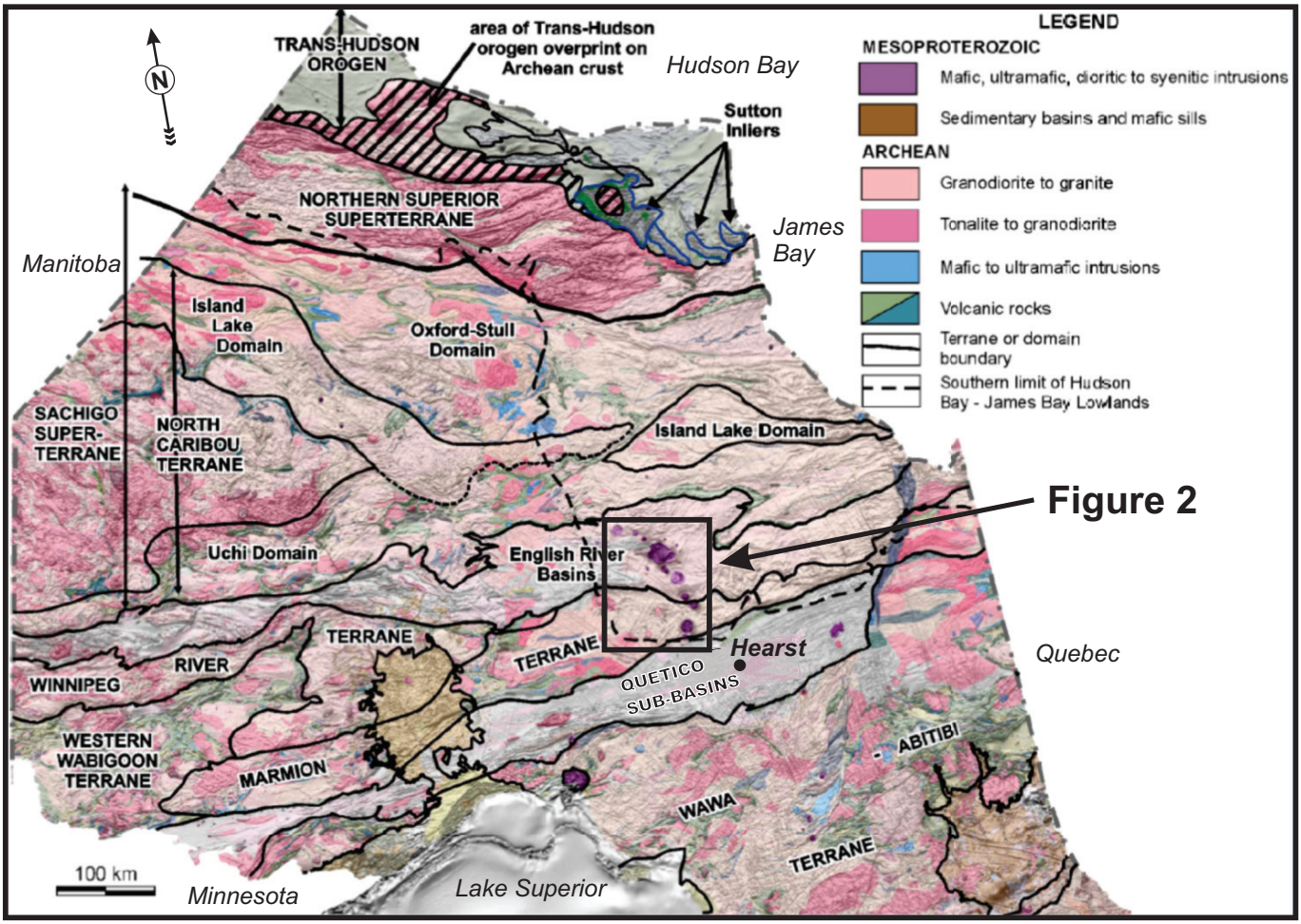

Fig. 1. Terrane boundary map of the Superior Province in Ontario (from Stott, 2011).

monzonite predominating. In contrast, the NRAC consists of fine- to coarse-grained amphibole-pyroxene syenite and lesser coarse-grained nepheline-bearing syenite and pegmatitic syenite, and minor granite (Sage, 1988).

The East (Fig. 5a) and West (Fig. 5b) pipes consist of angular to sub-rounded, millimetre- to metre-scale clasts. The clasts are mainly from the Albany complex, but fragments of amphibole-biotite schist, tourmaline-bearing granite, granite and gneiss, similar to rocks in the Marmion terrane and Quectico sub-province are common. Although sparse, brecciated fragments of semi-massive to massive graphite + silicate minerals occur in both pipes (Fig. 5c). The matrix consists of fine-grained (<0.5 mm) silicate minerals, which typically occur as discrete crystals and small monomineralic to polycrystalline aggregates intermixed with graphite (Fig. 6a). Matrix silicates tend to be angular to subangular and consist mainly of albite (30-60 modal%), perthitic feldspar (<40 modal%) and quartz (<25 modal%; Fig. 6a). Quartz crystals commonly display a polygonal fracture pattern (Fig. 6b). Finely disseminated solitary crystals and crystal aggregates of pyrite-pyrrhotite and magnetite are also observed in the matrix (Fig. 7a) and less commonly in fragments. The sulphide-oxide assemblage comprises less than 3 modal% of the rock, and typically <1 modal%. Discrete crystals of phlogopite and amphibole are rare win the matrix and local in lithic fragments. Hydrous silicate phases comprise <20 modal% of the rock.

A recently identified porphyritic monzodiorite/foid monzodiorite rock also forms breccias containing Albany complex clasts (Fig. 5d). This rock is spatially associated with, and closely, resembles, the graphite-bearing breccias but lacks graphite. Conly and Moore (2015) interpreted the rock as a hypabyssal, subvolcanic phase based on the occurrence of: 1) aphanitic groundmass consisting of albite, paragasite and minor nepheline; 2) embayed and sericitized albite xenocrysts with discontinuous, epitaxial overgrowths of sanidine; and 3) corona textured magmaclasts (consisting of a core of variably altered groundmass, an intermediate zone of subhedral to euhedral phlogopite and rimmed by anhedral to subhedal, radiating hastingsite ± phologopite). The hypabyssal phase is mainly distributed along the margins of the West pipe, but also occurs at depth (~400 m) along the outer margin of the East pipe, where it is cut by augite-aegirine syenite.

3.3. Mineralization and alteration

Graphite occurs both as intergranular (matrix) and intragranular (within lithoclasts) mineralization (Fig. 7a).

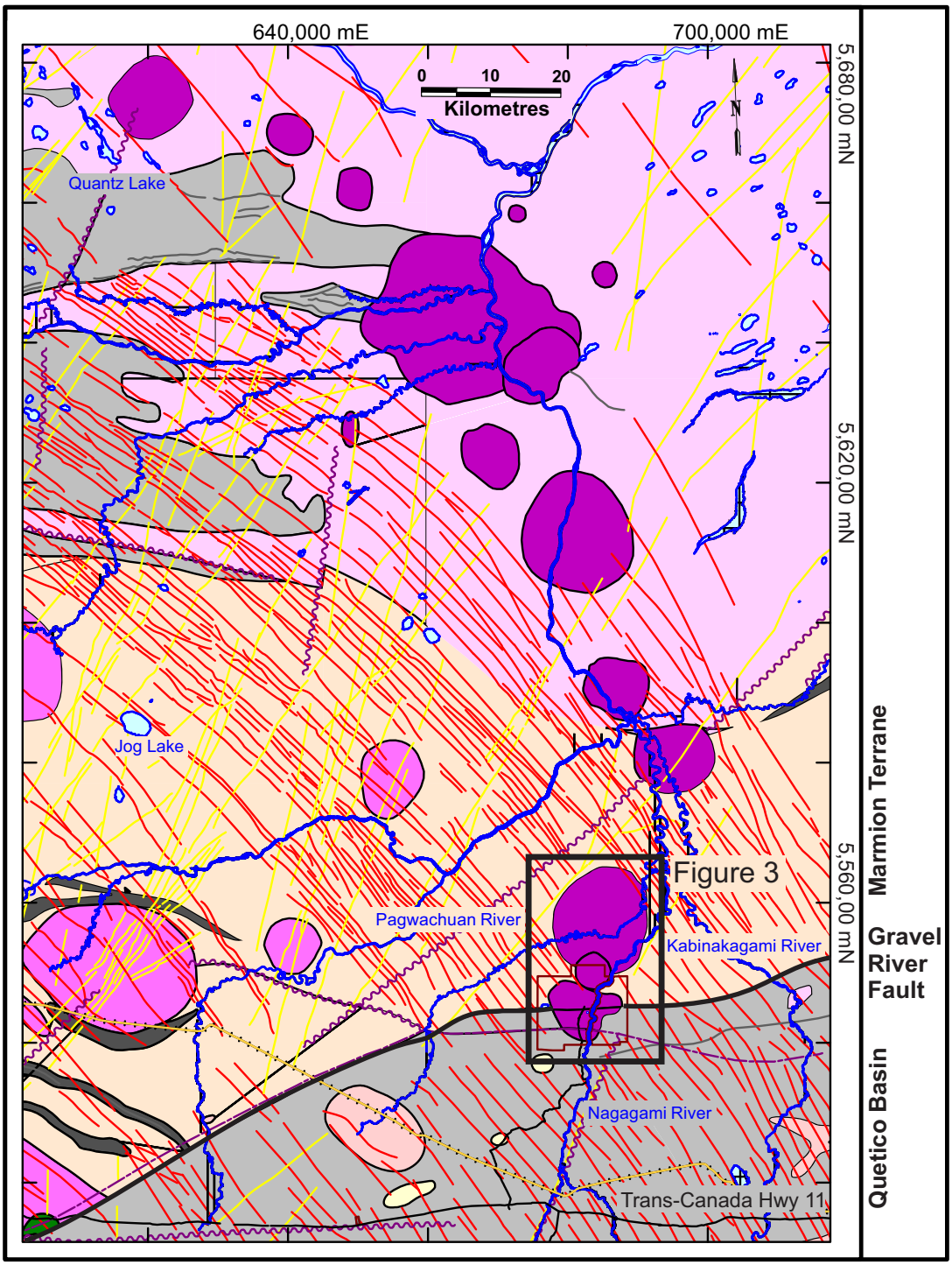

Fig. 2. Regional geology interpreted from aeromagnetic data (from Stott, 2008). UTM zone Z16, NAD 83.

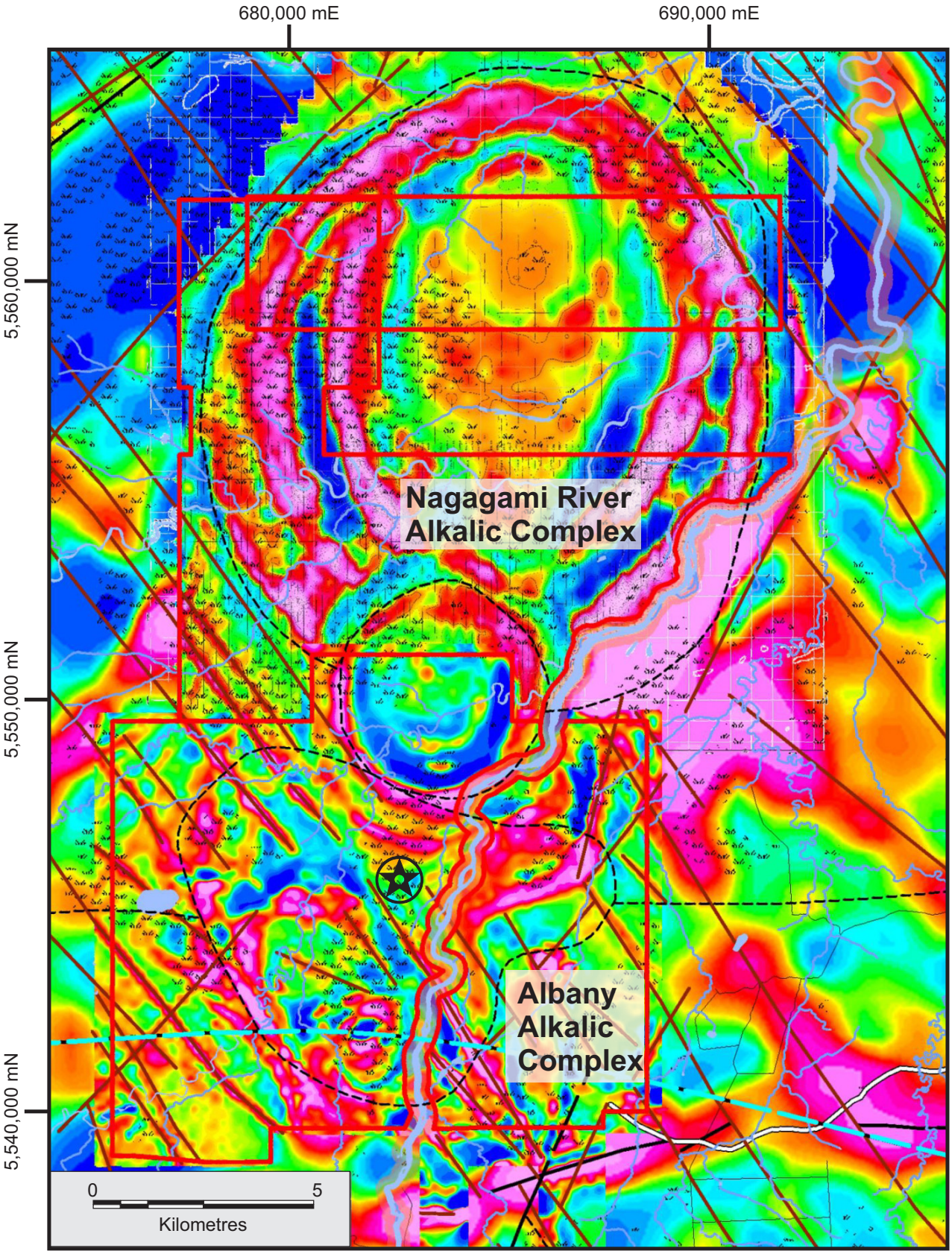

Fig. 3. Calculated vertical gradient aeromagnetic (composite) map of the Nagagami River Alkalic complex and the Albany Alkalic complex (courtesy Zenyatta Ventures Ltd.). Magnetic data are from multiple datasets that have not been merged and levelled. Location of the Albany graphite deposit is marked with the star. UTM zone Z16, NAD 83.

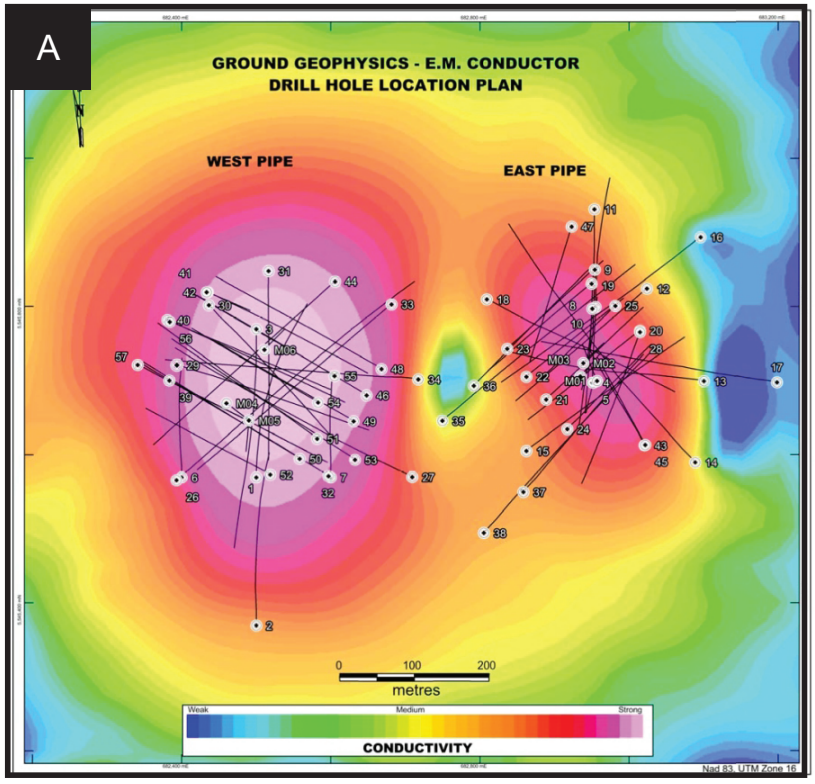

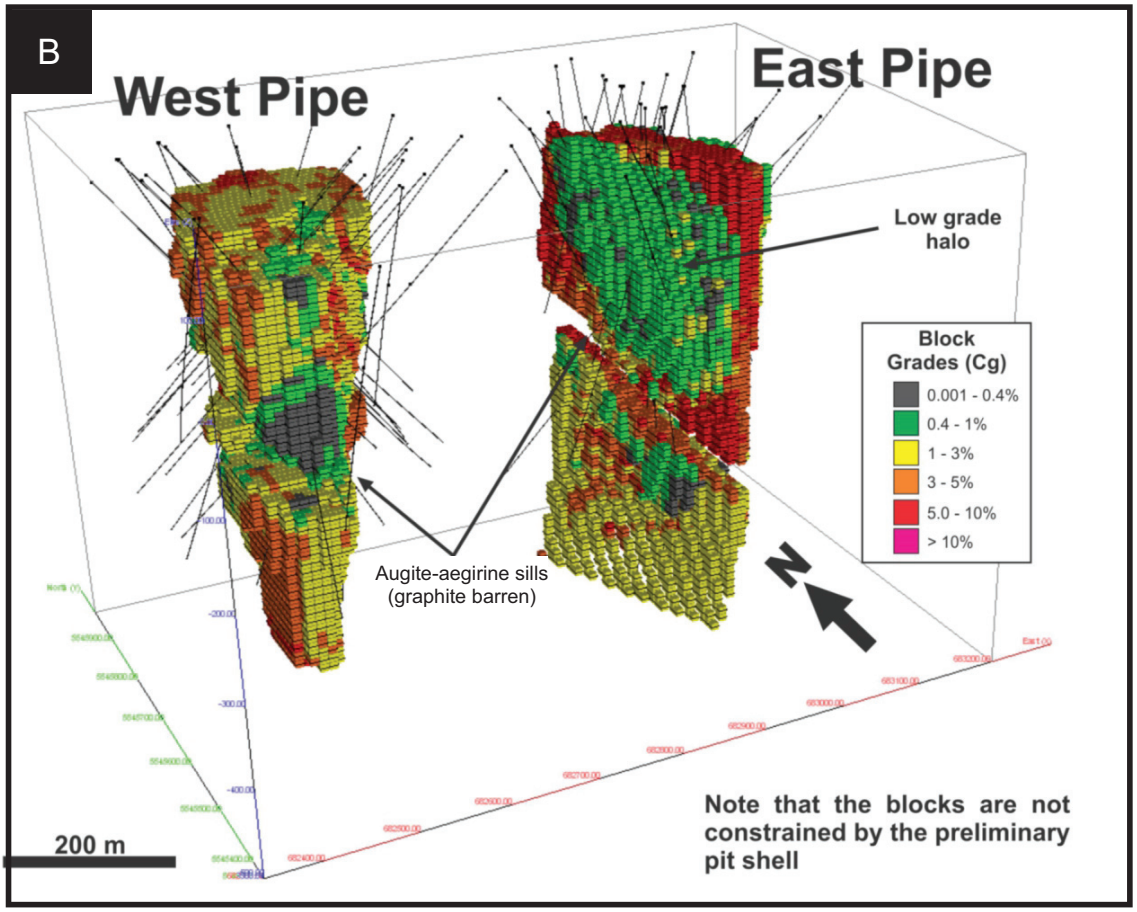

Fig. 4. a) Results of ground TDEM survey and drillhole locations and projections. **b)** 3-D block model of graphite grades, showing the pipe-like geometry of the Albany graphite deposit (both images courtesy of Zenyatta Ventures Ltd.).

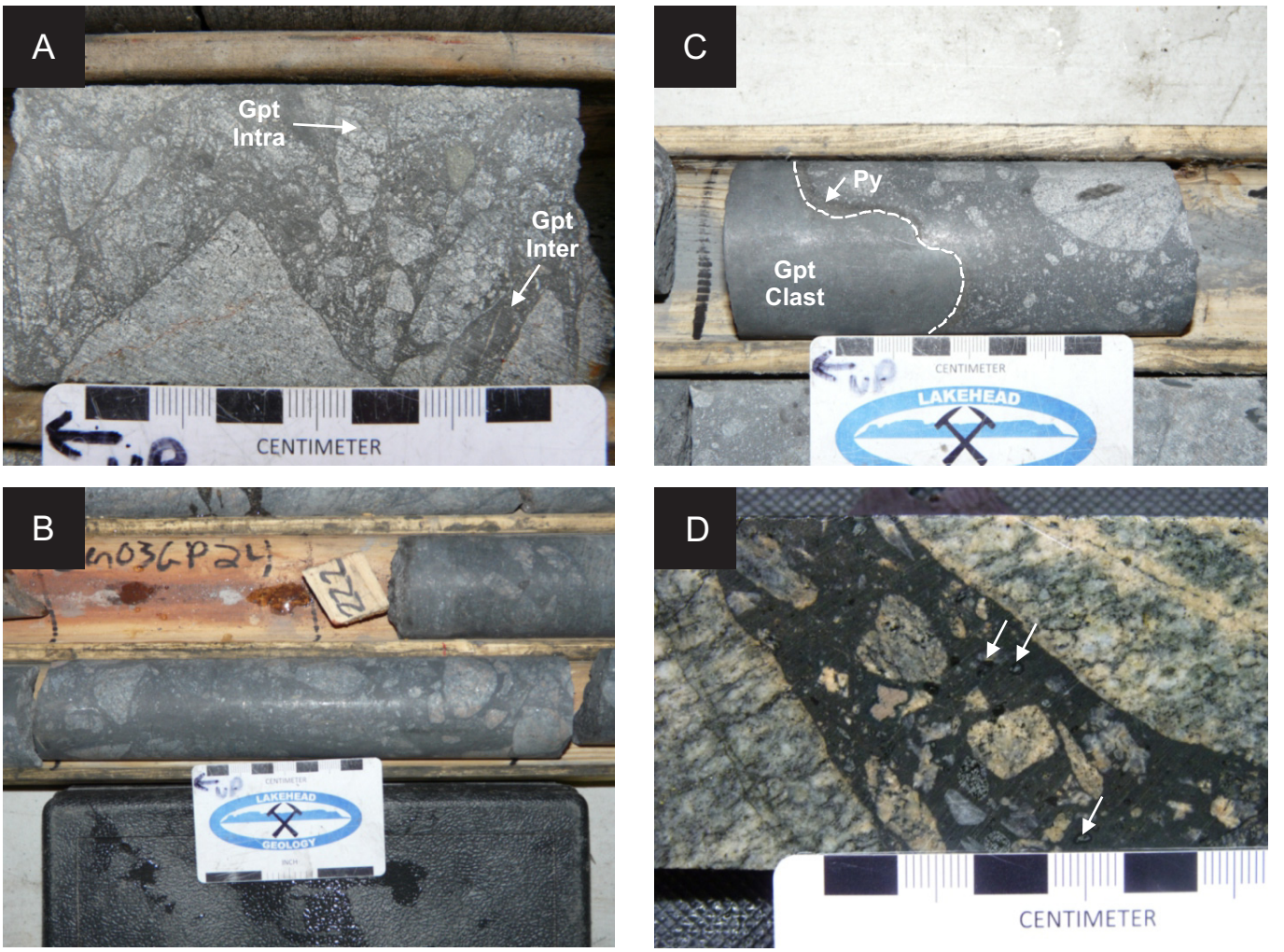

Fig. 5. Drill core photographs illustrating the typical breccia textures: **a)** East pipe with graphitic overprinting due to increased abundance of intragranular graphite in the fragments. **b)** High grade zone (~10% Cg) in the West pipe, where graphite is primarily concentrated in the breccia matrix. **c)** Graphite + silicate fragment in graphite mineralized West pipe breccia. **d)** Hypabyssal monzodiorite with fragments of potassic altered Albany complex syenite (magmaclasts are denoted by arrows). Mineral abbreviations: Gpt Intra – intragranular graphite; Gpt Inter – intergranular (matrix graphite).

Intragranular graphite represents a penetrative mineralization distributed along crystal boundaries and microfractures within lithoclasts. This style of mineralization also extends into unbrecciated to weakly veined Albany complex rock, producing a graphitic halo extending around the pipes. The higher contained graphite of the East pipe relative to the West pipe (with an indicated resource of 10.0 Mt at 5.60% C_g for the East pipe versus 14.3 Mt at 2.85% C_g for the West pipe; RPA Inc., 2015), is due to the development of a more extensive halo and a greater abundance of intragranular graphite in brecciated fragments (Fig. 5a). In the pipe halo, graphite also occurs as discrete millimetre- to centimetre-scale veins that increase in frequency towards the pipes. Matrix, graphite forms discrete laths, aggregated laths, mantles enclosing silicate crystals and lithofragments, and brecciated graphite+silicate fragments intermixed with finely fragmented silicates (Fig. 7b).

The breccias are essentially unmetamorphosed. Weak to extensive sericitization of plagioclase feldspar is the only ubiquitous alteration (Fig. 8a). Pyrite ± pyrrhotite alteration (Fig. 8b) is highly variable and consists mainly of finely disseminated crystals associated with matrix graphite and magnetite, and extends a few metres to several tens of metres beyond the graphitic halo. More discernable forms of this alteration assemblage occur as discontinuous sulphide rims along the edges of graphite+silicate fragments or encompassing graphite-rich regions of the matrix. Less common and highly localized types of alteration include phlogopite and hematite. Phlogopite alteration (Fig. 8c) is generally restricted to along matrix-clast contacts of fragments that contain a high degree of intragranular graphite mineralization ± sulphide alteration. Hematite alteration is rare and localized to the cores of sericitized feldspar crystals (Fig. 8d).

Supergene alteration is related to the development of the unconformity between the breccias and the overlying Paleozoic carbonate rocks. The supergene zone is highly variable in thickness and rarely extends into the breccias by more than

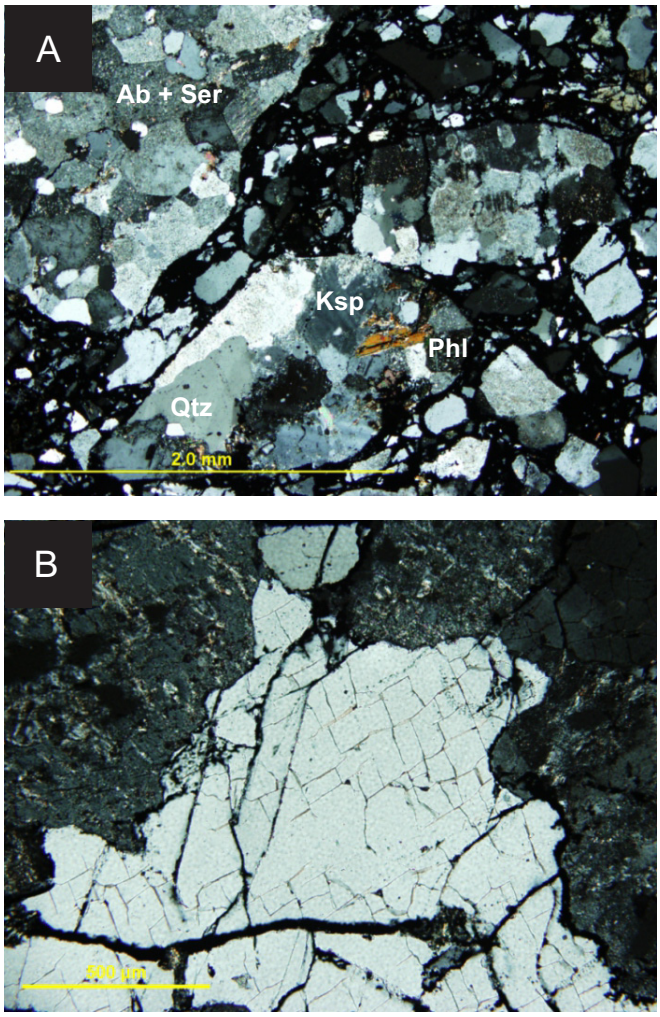

Fig. 6. a) Photomicrograph of the principle breccia mineral assemblage of plagioclase-potassium feldspar (perthitic)-quartz, with rare matrix phlogopite (cross-polarized, transmitted light). **b)** Quartz with well-developed, polygonal fracture pattern (cross-polarized, transmitted light). Mineral abbreviations: Qtz – quartz; Ab – albite; Ksp – potassium (perthitic) feldspar; Ser – sericite (muscovite) alteration; Phl – phlogopite.

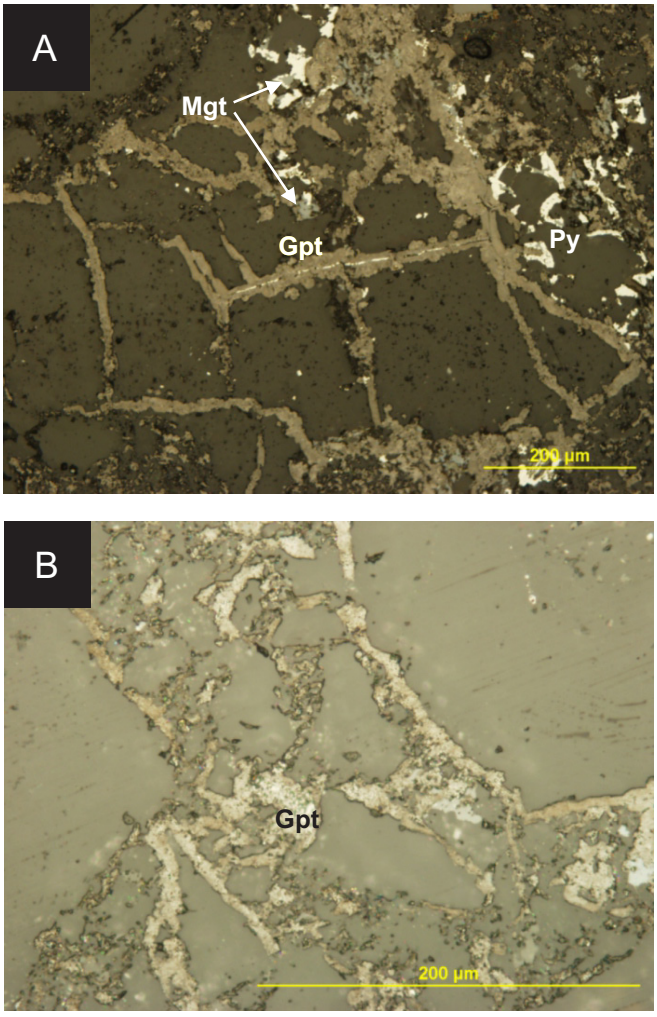

Fig. 7. Reflected light photomicrographs showing the textural differences between **a)** intragranular graphite and **b)** intergranular (matrix) graphite. Mineral abbreviations: Gpt – graphite; Mgt – magnetite; Py – pyrite.

30 m. Supergene alteration is poorly developed within non-brecciated and graphite mineralized Albany complex rocks. The supergene zone is most readily recognized by its hematite overprint and carbonate veining, but is also characterized by weak to pervasive replacement of silicate minerals in the breccias by sericite and chlorite.

4. Graphite characteristics

4.1. Morphology

Intergranular and intragranular graphite in the Albany deposit occurs as elongated lath-shaped aggregates of platy graphite crystals. Crystals and crystal aggregates are up to 300 µm long and 50 µm wide; however, the average size of individual crystals is <100 µm. Crystals are typically randomly orientated, as controlled by the orientation of breccia fragments, silicate crystal boundaries, and veins. There are, however, rare occurrences of well-foliated massive graphite in the breccias.

4.2. X-ray and Raman characteristics

X-ray diffraction of high purity concentrates (>99.9% C_g) of Albany graphite show that the graphite mineralization consists almost exclusively of hexagonal graphite (also called graphite alpha; Fig. 9a). Identification the hexagonal form is based on the position and symmetry of the peaks for (002) and (004) (planar) lattice planes. The *d*-spacing of the (002) plane of Albany graphite is 3.360 Å, with unit cell dimensions of a = 2.459 Å and c = 6.672 Å; consistent with highly ordered hexagonal graphite. The symmetry of the planar x-ray peaks and absence of discrete peaks for (101) and (012) prismatic lattice planes of rhombohedral graphite (also called graphite beta) at ~43.4 and ~46.3°2θ, respectively, indicates that Albany graphite lacks a rhombohedral phase. However, Albany graphite is characterized by a broad peak between 42.5 and 46.5°2θ, which overlaps with key prismatic peaks for hexagonal and rhombohedral forms of graphite (Fig. 9b). The peak characteristics observed for Albany graphite over this angular range are consistent with the development

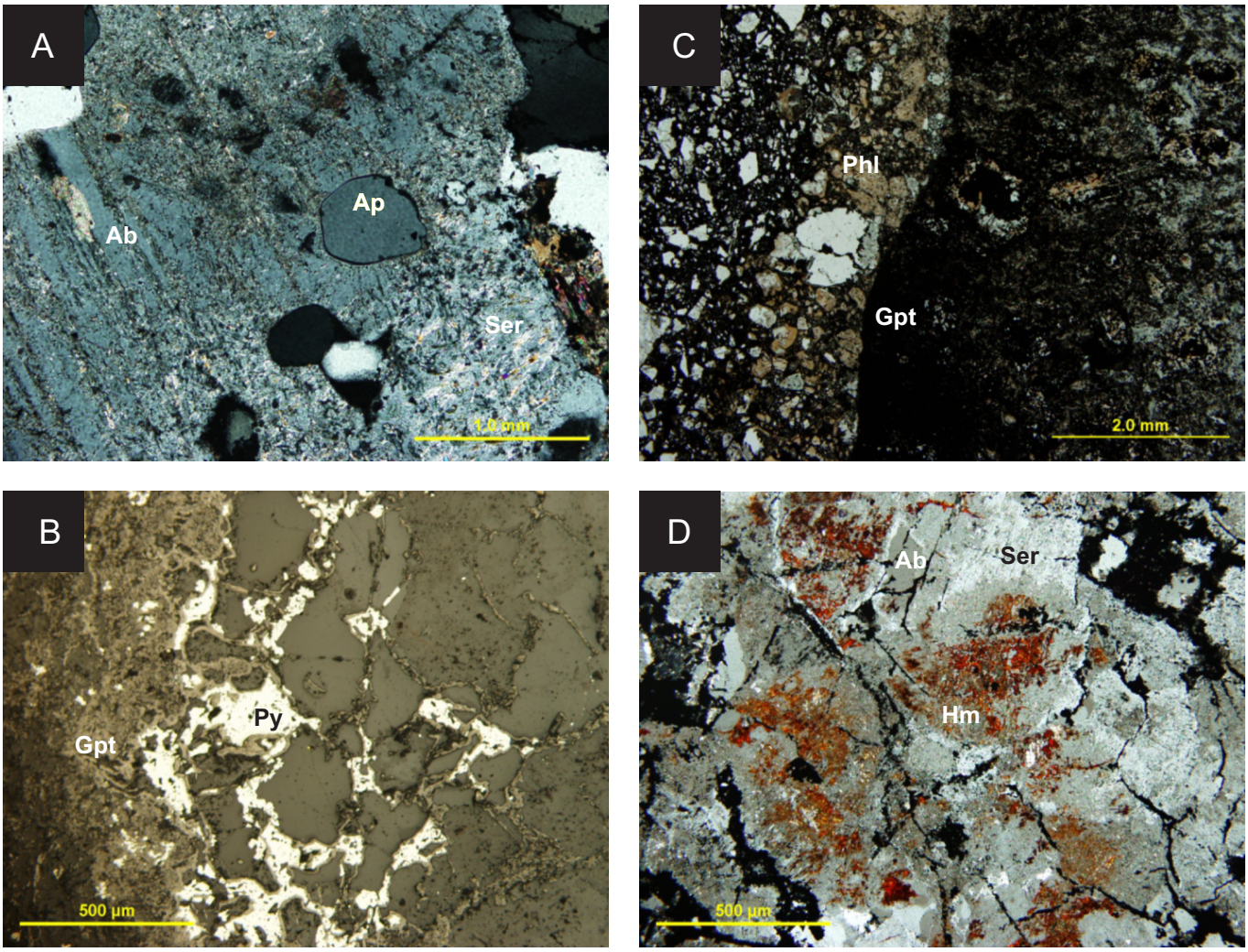

Fig. 8. Photomicrographs of the most common alteration types. **a)** Sericitization of plagioclase (cross-polarized, transmitted light). **b)** Pyrite, with graphite, forming along crystal contacts within a brecciate AAC fragment along the contact with matrix graphite (reflected light). **c)** Phlogopite rimming a graphitized Albany complex fragment (cross-polarized, transmitted light). **d)** Hematite alteration in the cores of plagioclase crystals. Mineral abbreviations: Ab – albite; Ap – apatite; Gpt – graphite; Hem – hematite; Ser – sericite (muscovite); Phl – phlogopite; Py – pyrite.

of turbostratic graphite. Similar to rhombohedral graphite, turbostratic graphite is a conversion of hexagonal graphite by mechanical modification, and results in random structural changes that may include rotation, translation, curvature and variation of interlayer spacing of graphene layers (e.g., Li et al., 2007). However, determining the specific structural changes associated with turbostratic development is not easily accomplished by XRD analysis.

Raman spectrum of graphite is composed of first-order (1100–1800 cm^{-1}) and second-order (2500–3100 cm^{-1}) regions (Tuinstra & Koenig, 1970; Nemanich & Solin, 1979). In the first-order region (Fig. 10a), the graphite band (G band) occurs at ~1580 cm^{-1} and corresponds to in-plane vibration of carbons in the graphitic structure. Bands occurring at 1350 cm^{-1} (D1 band) and 1620 cm^{-1} band (D2 band) correspond to defects in the graphitic structure and occur in poorly ordered graphite. As intensity and broadening of the D1 and D2 bands increase, the degree of ordering of the graphite crystal structure decreases. The degree of ordering can be assessed from the D1/G peak intensity ratio and D1/(D1+G+D2) peak area ratio. However, crystals must be selected with caution, as the Raman effect is dependent on crystal orientation and crystal size. For graphite, accurate Raman analyses must be performed on crystals that are orientated perpendicular to the crystallographic c-axis. Whereas loose powders can be preferentially orientated, in situ measurements from thin sections are more challenging. The D1/G ratio of Albany graphite measured in situ does vary greatly due to variances in crystal orientation. However, euhedral, hexagonal crystals with a high reflectivity are near to the ideal orientation, and yield a minimum D1/G ratio and a D1/(D1+G+D2) peak area ratio of 0.095 and 0.135, respectively, for Albany graphite. The Raman results for Albany graphite are comparable to synthetic, lithium-ion-grade graphite (D1/G = 0.102 ratio and D1/(D1+G+D2) = 0.193), and indicate a well-ordered crystal structure (Fig. 10b). The low intensity and wide band at 1500 cm^{-1} (D3 band) is also observed in some Raman

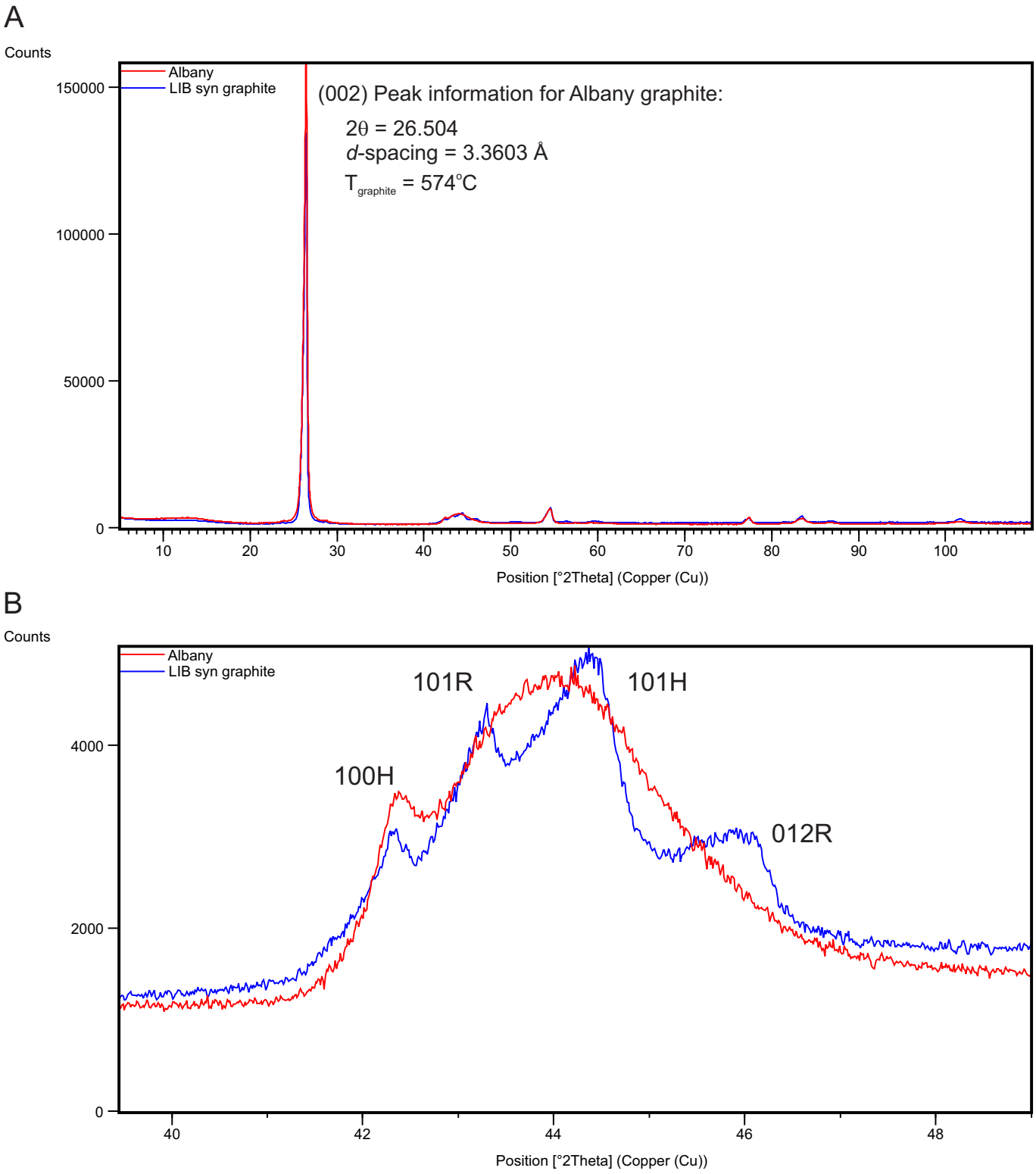

Fig. 9. X-ray diffraction patterns for Albany graphite concentrate (red) and synthetic, lithium-ion battery-grade graphite (blue). **a)** XRD patterns for the full scan range from 5 to 115º2θ. **b)** XRD patterns from the range between 40 and 48º2θ illustrating the difference in XRD profiles for turbostatic graphite (Albany) and rhombohedral graphite (synthetic graphite). Miller indices for key peaks are: H, hexagonal graphite, and R, rhombohedral graphite.

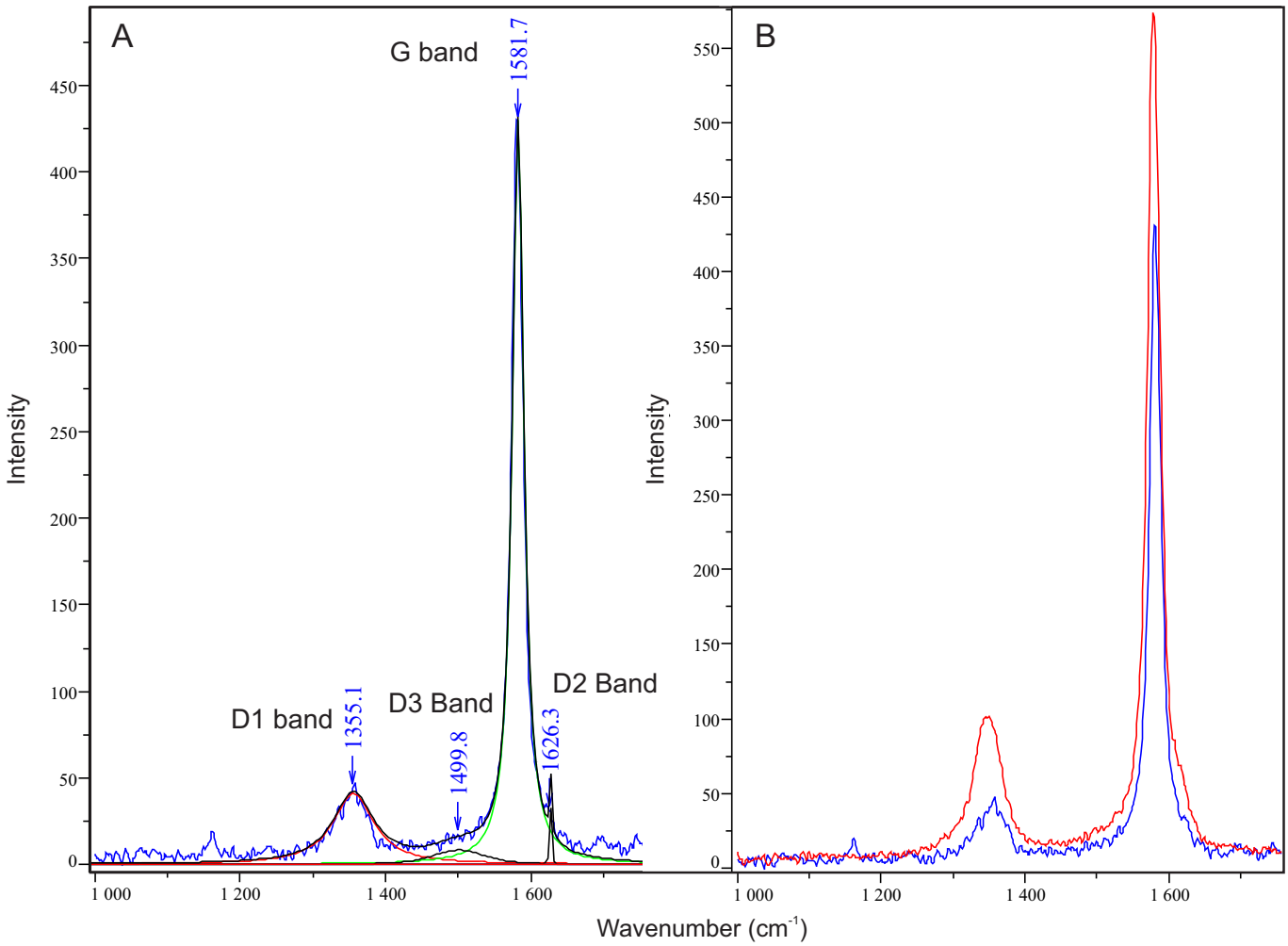

Fig. 10. a) Raman spectrum (first-order region) of an individual Albany graphite crystal aggregate aligned perpendicular to the crystallographic c-axis, yielding a D1/G peak intensity ratio of 0.95 and a Di/(D1+G+D2) peak area ratio of 0.135, corresponding to a temperature of crystallization of 581°C. **b)** Comparison of Raman spectra of Albany graphite (blue, same spectrum as in a) and synthetic, lithium-ion battery-grade graphite (red). The synthetic graphite samples yields a D1/G peak intensity of 0.102 and a Di/(D1+G+D2) peak area ratio of 0.193.

spectra of Albany graphite. The occurrence of the D3 band may reflect a poorly ordered form of carbon or it can be attributed to small crystallite sizes. This band is generally absent in graphite that has crystallized or undergone temperatures in excess of 400 to 450°C (Beyssac et al., 2002), and for this reason we attribute the manifestation of the D3 band in some Albany samples to small crystallite sizes (Nemanich and Solin, 1979).

The temperature of graphite crystallization can be estimated using XRD and Raman spectroscopy geothermometers. The graphite geothermometer of Shengelia et al. (1979) bases temperature estimates on the *d*-spacing of the (002) lattice plane. XRD-determined temperatures of high-purity Albany concentrate indicate an average crystallization temperature of 574°C. Unlike XRD, Raman spectroscopic methods have the advantage of being able to make in situ temperature estimates on individual crystals and crystal aggregates. The Raman geothermometer of Beyssac et al. (2002) uses the ratio of the peak area for first-order D and G bands to estimate crystallization temperature. Raman geothermometry of Albany samples yields a maximum crystallization temperature of 581°C. The temperature determinations are in good agreement with each other, and are within the ±20 to 50°C error for both geothermometers.

4.3. Carbon isotopic composition

Stable carbon isotope compositions for two high-purity concentrates from the East pipe are -16.9 and -16.8‰ (unpublished data). The $\delta^{13}C$ ratio of Albany graphite is intermediate between isotopically enriched sources, including mantle carbon ($\delta^{13}C \approx$ -7‰) and marine carbonates ($\delta^{13}C$ = 0 ± 2‰), and isotopically depleted organic matter ($\delta^{13}C$ = -40 to -6‰, average $\delta^{13}C$ = -25‰).

5. Genetic considerations

We interpret that the Albany graphite deposit is a rare example of crystalline graphite that formed in a shallow subvolcanic environment. Although the Albany deposit shares genetic attributes with other igneous-hosted, fluid-derived

deposits (e.g., Borrowdale, UK; Ortega et al., 2010), we consider that Albany represents a new-end member of igneous-hosted fluid-derived graphite. To the best of our knowledge the graphite-bearing conical breccia pipes are a unique attribute. We interpret the deposit to have formed during brecciation that was induced by the ascent of carbon-rich fluids that separated from alkalic magmas at depth.

5.1. Origin of the carbon and graphite precipitation mechanisms

Possible carbon sources include: 1) carbon-rich volatiles released from coeval magmas; 2) devolatilzation of carbonaceous country rock; and 3) assimilation of carbonaceous country rock. The carbon isotopic ratio of Albany graphite could readily be explained by binary mixing of a carbonaceous fluid phase that segregated from a mantle-derived melt and carbon-derived from metasedimentary country rock (such has been described from, for example, New Hampshire; Ruby Range, Montana; Black Hills, South Dakota; Huelma, Spain; Borrowdale, UK; see Luque et al., 2012, and references therein). However, Quetico sub-province rocks are relatively carbon-poor (P. Fralick, per. comm., 2014) and are, therefore, unlikely to have provided sufficient carbon.

We postulate that graphite precipitated from an orthomagmatic carbon-rich (CO_2-CH_4-H_2O ± H_2S) fluid in response to near surface magma degassing. The specific carbon species composition of the mineralizing fluid is unknown, as suitable fluid inclusions have not been identified. Nonetheless possible graphite forming reactions can be postulated using mineralogical constraints and the carbon isotope composition of Albany graphite. Direct precipitation of graphite from a CO_2-bearing orthomagmatic fluid ($CO_2 \rightarrow C + O_2$) is unlikely because reduction of CO_2 by the co-precipitation of a Fe^{3+}-bearing phase is necessary. Although magnetite co-exists with graphite, the quantity of magnetite (trace to 2 modal%) is likely insufficient to drive the required changes in the f_{O2} of the fluid to induce graphite precipitation directly from CO_2.

An alternative reaction for graphite precipitation from a fluid that is initially CO_2-bearing is:

$$CO_2 + 2H_2 \rightarrow C + 2H_2O$$

We favour that the initial fluid was CO_2-rich, in contrast to a CH_4-rich fluid, as the former species occurs in much greater pre-eruptive concentrations over a range of magma compositions (e.g., Wallace et al., 2002). The above reaction can be re-expressed as a Fischer-Tropsch reaction (e.g., Salvi and Williams-Jones, 1997) where:

$$CO_2 + 4H_2 \rightarrow CH_4 + 2H_2O$$

With the subsequent precipitation of graphite by:

$$CO_2 + CH_4 \rightarrow 2C + 2H_2O$$

or

$$CH_4 + O_2 \rightarrow C + 2H_2O$$

Fischer-Tropsch synthesis results in the precipitation of graphite with a $\delta^{13}C$ = -16.9‰, which is identical to the composition of Albany graphite concentrates, by equilibrium fractionation at 574°C (= XRD determined maximum temperature), assuming an initial $\delta^{13}C_{CO2}$ of -7.5‰ (= mantle) and $\Delta^{13}C_{CO2\text{-}CH4}$ = 13.2‰, $\Delta^{13}C_{graphite\text{-}CH4}$ = 3.4‰ and $\Delta^{13}C_{CO2\text{-}C}$ = 9.4‰ (Bottinga, 1969).

5.2. Role of hypabyssal (subvolanic magmas)

As indicated in the above reactions, Fischer-Tropsch synthesis of graphite-forming hydrocarbons requires the addition of H_2 to ultimately generate graphite. Hydrogen can be derived through various wall-rock alteration reactions involving a precursor hydrous mineral phase (e.g., Salvi and Williams-Jones, 1997). However, interaction between an orthomagmatic fluid and Albany rocks is unlikely to have generated sufficient quantities of H_2, owing to the main plagioclase-potassium feldspar-quartz assemblage and lack of metasomatic reactions involving precursor hydrogen-bearing phases (mica, amphibole). Conly and Moore (2015) proposed H_2 generation at Albany in response to hydrous crystallization (e.g., Beard et al., 2005) associated with magmaclast paragenesis of the hypabyssal, subvolcanic monzonite, via the following reactions:

Hydrous monzonite melt + Diopside + Fe-Ti oxides + Ca-plagioclase →
Hastingsite + Albite + $Melt_{(groundmass)}$ + F-bearing fluid

With subsequent replacement of hastingsite by phlogopite:

Hastingsite + F-bearing fluid →
Phlogopite + Apatite + Quartz + $Fe^{3+}_{(aq)}$ + $Na^{+}_{(aq)}$ + H_2O

And H_2 produced via:

$$Fe^{3+}_{(aq)} + H_2O \rightarrow Fe(OH)_2^{+} + H_2$$

The last two reactions also provide the fluid constituents necessary for the alteration types (sericite and hematite) observed in the graphitic breccias.

5.3. Genetic model

We propose a four-stage genetic model for the Albany deposit. The first stage corresponds to pre- and syn-mineralization events necessary to form the host rocks and generate the carbon-rich fluids from which graphite precipitated. The second and third stages include the development of the breccia pipes, segregation of a carbon-rich fluid from ascending hypabyssal magmas, and the eventual precipitation of graphite. The final stage details post-ore events.

5.3.1. Stage 1: pre- to syn-mineralization magmatic events

Emplacement of the Albany breccia pipes is estimated to be Mesoproterozoic to Neoproterozic, based on cross-cutting

relationships with the Paleoproterozoic Matachewan (Hearst) and Kapuskasing dike swarms (Fig. 2).

Emplacement of the hypabyssal monzodiorite and, possibly, the NRAC may have coincided with graphite formation. Our preliminary strontium isotope results show that present-day $^{87}Sr/^{86}Sr$ ratios for the hypabyssal monzodiorite (0.71497-0.730232) and Nagagami River complex (0.730509-0.733026) are significantly less radiogenic then the Albany complex (0.740247-0.819211). The similarity in $^{87}Sr/^{86}Sr$ ratios for the hypabyssal monzodiorite and Nagagami River complex indicate that these two may be petrogenetically related. A mantle origin is plausible considering the depleted strontium isotope composition relative to other igneous units associated with the deposit.

5.3.2. Stage 2: orthomagmatic fluid generation and breccia pipe development

Degassing of the postulated hypabyssal magma and subsequent segregation of a CO_2-bearing fluid was in response to the depressurization of the ascending magma at mid- to shallow-crustal levels, wherein CO_2 accumulated at the top of the ascending hypabyssal monzodiorite dike. Continued ascent to shallower crustal levels may have resulted in continued fracturing of the country rock and production breccia, due to decreasing overburden pressure. The co-existence of angular and rounded breccia fragments is evidence of mixing of juvenile fragments and records different amounts of mechanical abrasion.

5.3.3. Stage 3: graphite deposition

Pressure and temperature changes associated with dike accent during Stage 2 would have been insufficient to induce graphite mineralization or crystallization of the hypabyssal magma (i.e., supercritical CO_2 fluid and above liquidus temperature would have persisted). Consequently, graphite deposition is restricted to shallower crustal levels and occurred in response to decreases in pressure and temperature. We propose that graphite deposition occurred rapidly due to sudden depressurization and quenching (from supercritical to gas) of the CO_2-fluid in response to the dike head breaking the surface and venting CO_2 gas. The fine crystal size of Albany graphite and high abundances of discrete crystals and fine crystal aggregates are consistent with rapid changes in pressure-temperature conditions, which would have inhibited growth of coarser-crystalline graphite. We estimate formation within two kilometres of the paleosurface. The graphite mineralization is known to currently extend below 500 m, and underlie the two large barren sill complexes beneath the deposit (Fig. 4). The sudden pressure and temperature change would have also induced hydrous crystallization of the hypabyssal monzodiorite magma, resulting in H_2 gas generation necessary for Fischer-Tropsch synthesis. The aphanitic component of the mozondiorite is additional evidence for rapid cooling in the pipes.

5.3.4. Stage 4: post-mineralization magmatic and erosional events

Post-mineralization events include: 1) emplacement of late-stage augite-aegirine syenite; 2) intrusion of aplite and other felsic dikes; 3) erosion of upper levels of the AAC complex and supergene alteration; and 4) deposition of Paleozoic carbonate rocks and Quaternary glacial sediments.

6. Conclusions

The Albany deposit is a unique type of igneous-hosted, fluid-derived graphite mineralization. Igneous-hosted deposits are rare, as these environments do not usually provide suitable conditions for the formation of sizable deposits. The defining characteristic of the Albany deposit is the occurrence of crystalline, fine-grained graphite within two large breccia pipes. The formation of the Albany deposit required an unusual combination of geological factors, including: 1) intrusion of CO_2-rich hypabyssal monzondiorite magmas, of possible mantle origin; 2) generation of a CO_2-CH_4 orthomagmatic fluid by Fischer-Tropsch synthesis; 3) development of two vent breccia pipes due to turbulent ascent of a gas-rich orthomagmatic fluid; and 4) precipitation of graphite in response to the sudden depressurization and quenching of the orthomagmatic fluid. The rapid precipitation of graphite at temperatures up to 581°C generated fine grained, but highly crystalline graphite, with comparable crystallographic properties to synthetic graphite used in the manufacturing of lithium-ion batteries.

Acknowledgments

This study is a collaboration between Lakehead University and Zenyatta Ventures Ltd., and is funded by the Natural Sciences and Engineering Research Council of Canada (grant number CRDPJ 458909-13).

References cited

Beard, J.S., Ragland, P.C., and Crawford, M.L., 2005. Using incongruent equilibrium hydration reactions to model latter-stage crystallization in plutons: Examples from the Bell Island Tonalite, Alaska. Journal of Geology, 113, 589–599.

Beyssac, O., Goffe, B., Chopin, C., and Rouzaud, J.N., 2002. Raman spectra of carbonaceous material in metasediments: a new geothermometer Journal of Metamorphic Geology, 20, 859–871.

Bottinga, Y., 1969. Calculated fractionation factors for carbon and hydrogen isotope exchange in the system calcite-carbon dioxide-graphite-methane-hydrogen-water vapor. Geochimica et Cosmochimica Acta, 33, 49-64.

Conly, A.G., and Moore, L.C., 2015. Role of hypabyssal subvolcanic magmas in the genesis of the Albany graphite deposit: Joint Assembly (GAC-MAC-AGU) 2015 Program with Abstracts, Abstract number MD34A-0201 (web accessed May 25, 2015).

Heaman, L.M., 1988. A precise U-Pb zircon age for a Hearst dike. In Program with Abstracts, Annual Meeting Geological Association of Canada-Mineralogical Association of Canada, 13, A53.

Johnson, M.D, Armstong, D.K., Sandord, B.V., Telford, P.G. and Rutka, M.A., 1991. Paleozoic and Mesozoic Geology of Ontario. In Geology of Ontario, Ontario Geological Survey, Special Volume 4, Part 1, pp. 383-403.

Kennedy, M.C., 1984. The Quetico Fault in the Superior Province of the southern Canadian shield. Unpublished MSc thesis, Lakehead

University, Thunder Bay, Ontario, 300p.
Legault, J.M., Lymburner, J., Ralph, K., Wood, P., Orta, M. and Prikhodko, A., 2015. The Albany graphite discovery airborne and ground time-domain EM. KEGS Geophysics Symposium, Society of Economic Geophysicists Technical Program Expanded Abstracts 2015, pp. 2056-2060.
Li, Z.Q., Lu, C.J., Xia, Z.P., Zhou,Y., and Luo, Z., 2007. X-ray diffraction patterns of graphite and turbostratic carbon. Carbon, 45, 1686–1695.
Luque, F.J., Crespo-Feo, E., Barrenechea, J.F., and Ortega, L., 2012. Carbon isotopes of graphite: Implications on fluid history. Geoscience Frontiers, 3, 197-207.
Luque, F.J., Huizenga, J-M., Crespo-Feo, E., Wada, H., Ortega, L. and Barrenechea, J. F., 2013. Vein graphite deposits: geological settings, origin, and economic significance. Mineralium Deposita, 49, 261-277.
Nemanich, R.J., and Solin, S.A., 1979. First- and second-order Raman scattering from finite-size crystals of graphite. Physical Review B, 20, 392–401.
Ortega, L., Millward, D., Luque, F.J., Barrenechea, J.F., Beyssac, O., Huizenga, J.M., Rodas, M., and Clarke, S.M., 2010. The graphite deposit at Borrowdale (UK): a catastrophic mineralizing event associated with Ordovician magmatism. Geochimica et Cosmochimica Acta, 74, 2429–2449.
Phinney, W.C., and Morrison, D.A., 1988. Constraints on the environment of Matachewan dike intrusion. Abstract IGCP-257, International Symposium on Mafic Dikes and Related Magmatism, University of Lund, Sweden.
RPA Inc., 2015. Technical Report on the Preliminary economic assessment of the Albany graphite project, northern Ontario, Canada, prepared for Zenyatta Ventures Ltd., filed on SEDAR/ available at www.sedar.com (accessed August 21, 2015).
Sage, R.P., 1988. Geology of carbonatite - alkalic rock complexes in Ontario. Nagagami River Alkalic Rock Complex, District of Cochrane, Ontario Geological Survey, Study #43, 55 p.
Salvi, S., and Williams-Jones, A.E., 1997. Fischer-Tropsch synthesis of hydrocarbons during sub-solidus alteration of the Strange Lake peralkaline granite, Quebec/Labrador, Canada. Geochimica et Cosmochimica Acta, 61, 83-99.
Shengelia, D.M., Akhvlediani, R.A., and Ketskhoveli, D.N., 1979. The graphite geothermometer. Dokl. Acad. Nauk SSSR, 235, 132-134.
Stott, G.M., 2008. Precambrian geology of the Hudson Bay and James Bay lowlands region interpreted from aeromagnetic data – south sheet. Ontario Geological Survey, Preliminary Map P.3599, scale 1:500,000.
Stott, G.M., 2011. A revised terrane subdivision of the Superior Province in Ontario; Ontario Geological Survey, Miscellaneous Release—Data 278.
Tuinstra, F., and Koenig, J. L., 1970. Raman spectrum of graphite. Journal of Chemical Physics, 53, 1126–1130.
Wallace, P.J., Anderson Jr., A.T., Davis, A.M., 2002. Quantification of pre-eruptive exsolved gas contents in silicic magmas. Nature, 377, 612-616.